Temperature-dependent mobility modeling of GaN HEMTs by cellular automaton method

Koichi Fukuda
AIST
Tsukuba, Japan
https://orcid.org/0000-0002-3148-6010

Junichi Hattori
AIST
Tsukuba, Japan

Hidehiro Asai
AIST
Tsukuba, Japan

Junya Yaita
Fujitsu Limited
Atsugi, Japan

Junji Kotani
Fujitsu Limited
Atsugi, Japan

***Abstract*— GaN HEMTs are expected to achieve better device performance for microwave applications. The cellular automaton method is effective for predicting the transport characteristics of the two-dimensional electron gas, which is the key to the HEMT device performance. To predict the mobility of two-dimensional electron gas, it is necessary to consider the physics of the subbands. Since the traditional powerful Monte Carlo method selects the electron scattering mechanism by random numbers, it is necessary to suppress statistical problems to obtain a stable solution. We confirmed that our approach that combines the Poisson-Schrodinger and the cellular automaton method enables seamless and stable mobility calculations over a wide temperature range including low temperatures. In this paper, the temperature-dependent electron mobility of GaN HEMT calculated with and without interface roughness scattering model is studied.**

Keywords—GaN, HEMT, Poisson-Schrodinger, Cellular Automaton, electron mobility, interface roughness, two-dimensional electron gas

I. INTRODUCTION

As GaN HEMTs are becoming more successful in the microwave market, further improvements in their device performance are expected [1]. One of the important device performances of HEMT is the electron mobility of two-dimensional electron gas (2DEG). To predict the electron mobility of the HEMT hetero-structure, it is necessary to consider the inter-subband scattering that determines the electron charge balance of the subbands. In this field, the Poisson-Schrodinger Monte Carlo approach has been standard [2]. However, at low temperatures where phonon scattering decreases, the Monte Carlo approach, which treats the scattering phenomena by random numbers, requires additional efforts to avoid statistical problems. Moreover, the amount of carrier in each subband changes depending on the acceleration electric field, which should be considered accurately and seamlessly.

In the present method, which combines the Poisson Schrodinger and the cellular automaton method [3,4], the momentum distribution function of electrons is represented by a numerical table for each subband. The momentums of electrons are updated by small time-steps below a femtosecond. In this method, the electron scattering mechanism is not selected by using random numbers as in the Monte Carlo method, and the distribution function table is updated according to the scattering probability itself so that statistical fluctuations do not occur. This feature allows stable mobility calculation seamlessly even at low temperatures where phonon scattering becomes significantly low. In low-temperature conditions, the interface roughness scattering plays an important role. We applied the present method to the calculation of temperature-dependent mobility of GaN HEMTs because the low-temperature Hall mobility is often used to investigate experimentally the origin of scattering mechanisms that determine the mobility. The method clarifies the effects of scattering mechanisms on HEMT mobility, which is essential knowledge to design HEMT devices.

II. SIMULATION METHOD

Fig. 1 shows the concept of this method. Subbands are calculated by the Poisson-Schrodinger method. By providing a numerical table of two-dimensional electron momentum distribution function for each subband, it is possible to express the electron momentum distribution over wide orders of magnitudes. By applying electric field for electron acceleration in the other two dimensions, the numerical tables are updated by sub-femtosecond time-steps, and the time-dependent drift velocity and the mobility of the HEMT structure are obtained. The upper valleys are negligible for the low field electron mobility modeling, but not negligible for the high field drift velocity modeling. Depending on the hetero layer structure of HEMT, the energy difference between subbands may be small, and the mobility calculation may not be limited to the lowest subband even in low acceleration electric field conditions.

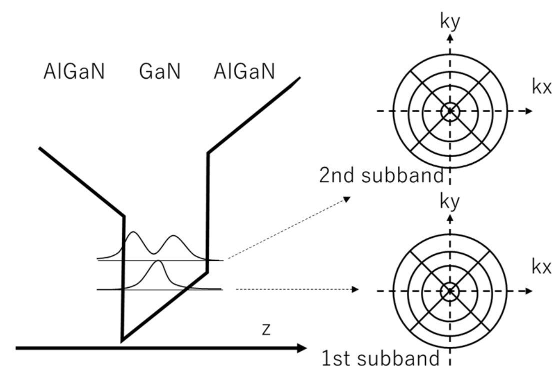

Fig. 1. Concepts of the present Poisson-Schrodinger and cellular automaton coupled method. Distribution function tables for 2D momentum spaces are prepared for each subband of each valley obtained by the Poisson-Schrodinger method applied to one-dimensional HEMT channel layer structures.

978-1-6654-0685-7/21/$31.00 ©2021 IEEE

Fig. 2 shows the calculation algorithm of this method. When the electron concentration of each subband changes due to inter-subband scattering, redistribution of the electron concentration is feedbacked to the Poisson-Schrodinger and is self-consistently solved. In the cellular automaton method, each momentum distribution function table is updated by the electric field acceleration and various scattering of electrons at each time step. For the scattering calculation, the overlap integral of the envelope function is used, which is the same as the Monte Carlo for 2DEG. For phonon scattering, acoustic phonons, non-polar optical phonons, and polar optical phonons were considered, and the parameters of the reported bulk GaN Monte Carlo were used [5,6]. For interface roughness scattering, a Gaussian-shaped surface scattering model, $\delta(r) = \Delta^2 \exp(-r^2/L^2)$, was used [7].

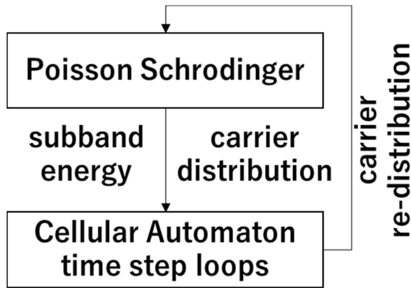

Fig. 2. Calculation flow of the present method. The distribution function tables are updated for each time step, corresponding to the acceleration by the electric field and the scattering of various mechanisms. The distribution function updated by the cellular automaton method is reused to update the carrier profiles and is feedbacked to the Poisson-Schrodinger solver to consider the carrier redistribution effects.

Fig. 3 shows the conceptual explanation of the distribution function update procedures for a) the field acceleration and b) the scattering. In the field acceleration, the distribution functions starting from the momentum mesh points move to the certain momentum endpoints between the mesh points, and the amounts of the distribution function are distributed to the momentum mesh points around the endpoint. For the scattering, the distribution function at each mesh point is divided into the momentum after the scattering proportional to the angular-dependent scattering probabilities. In b) the scattering is described as the elastic process but inelastic processes are also treated with the interpolation method described in ref. [9].

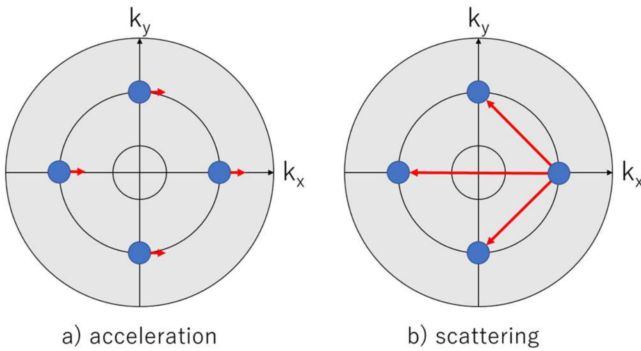

Fig. 3. Concept of the distribution function update for a) field acceleration and b) scattering in the present method.

Carrier concentrations can be extremely low at low temperatures, and some variables in the Poisson-Schrodinger method are treated as quadruple precision. Since most of the calculation time is in the cellular automaton part, the influence of the quadruple precision on the total calculation time is negligible. OpenMP parallelization was applied to the loop updating the distribution function table. The calculations of the overlap integral values to obtain the scattering probability are computationally heavy, but since they change slowly with the time step, the calculation time is saved by skipping the overlap integral calculation for certain time-steps. Total calculation time for 20 picosecond calculation of electron transport with 0.5 femtosecond time-steps, which means 40000 time-steps, is less than 10 minutes using 16-core OpenMP if only the first subband of the first valley is considered. If N-subbands are considered, calculation time is proportional to N^2 because of the inter-subband scattering calculations.

Drift velocities and mobilities are obtained directly from the momentum distribution function tables which represent weighted electron velocity distribution themselves. The momentum mesh should be minute enough for a numerically accurate calculation of the low field and the low-temperature conditions. The compatible drift overshoot characteristics to those calculated by the Monte Carlo method are already confirmed in the previous work [4]. As discussed in [4], the overshoot characteristics obtained by the present method are always smooth and stable, while the Monte Carlo requires more and more particles to reduce the statistical noises, especially for low-field conditions.

III. Simulation Results and Discussions

Fig. 4 shows the HEMT layer structure studied in this work. The Poisson-Schrodinger method is applied to the z-direction across the HEMT layer structure to obtain subband energies and eigenfunctions of the 2DEG. Initially, electron concentration profiles are obtained by assuming the Fermi-Dirac energy distribution. Interface charges induced by the hetero-layer strain are included in the Poisson equation. These charges determine the conduction band slope differences for both sides of the semiconductor interfaces, which critically influence the confinement of the 2DEG. The simulator calculates the electron transports of the 2DEG when an electric field is applied in the x-direction in the left figure of Fig. 4. In this paper, we focused on a structure in which the GaN channel is sandwiched between AlN layers.

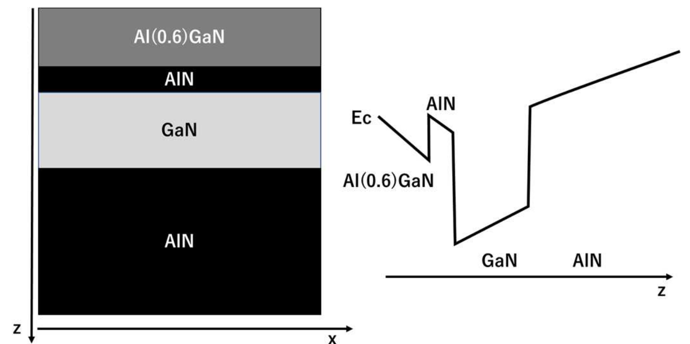

Fig. 4. Assumed AlN/GaN/AlN HEMT sandwich structure. Strain-induced charges are assumed at semiconductor interfaces.

Fig. 5 shows the calculated results in the cross-sectional depth profile of the HEMT layer structure with the GaN layer thickness of 30 nm. The black solid line shows the conduction band minimum profile on the right axis with the bottom energy of more than 0.5 eV below the Fermi-energy 0 eV at 8 nm depth. The electron concentration of each subband is shown by lines with markers on the left axis. In this case, the first subband electrons (red) are 5-orders of magnitude more than those in the second subband (green). The subband energies plus waves with the widths of the squared envelope functions are shown by the same color on the right axis. It should be noted that the first subband energy is 0.5 eV larger than the conduction band bottom because of the strong confinement. The conduction band is strongly bent around the AlN / GaN interface at 8 nm depth because of the induced first subband electron concentration around 10^{20} cm^{-3}.

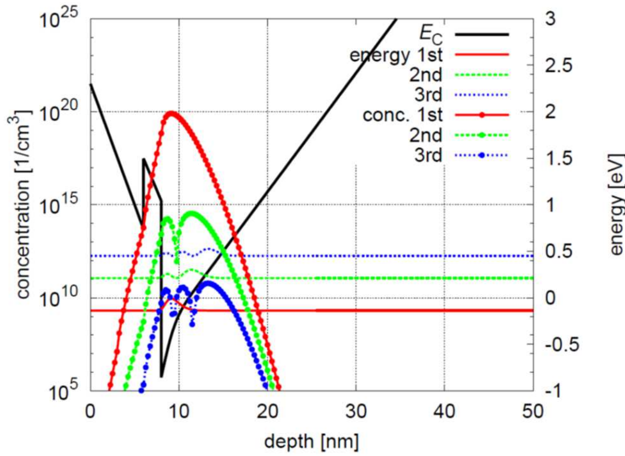

Fig. 5. The Poisson-Schrodinger results for the GaN channel thickness of 30 nm. The black line shows the conduction band minimum profile on the right axis. The 3-color lines with markers show the electron profile on the left axis. The 3-color lines without markers are subband energy with small waves corresponding to the squared eigenfunctions.

Fig. 6 shows time-dependent electron drift velocities when an electric field of 1 kV / cm is applied for three temperatures of 5 (blue), 77 (green), and 300 K (red). In these calculations, only phonon scatterings were considered, and overshoot characteristics with different time scales were obtained depending on the temperature. A stable solution is obtained by the present method even under low-temperature conditions with low scattering probabilities. The longer time drift velocity overshoot is observed in lower temperature conditions. For the room temperature, the drift velocity 2×10^6 cm/s is obtained which corresponds to the mobility of 2000 cm^2/Vs. This value is larger than the experimentally obtained mobility as in ref [8] because Fig. 5 is calculated without interface roughness scattering.

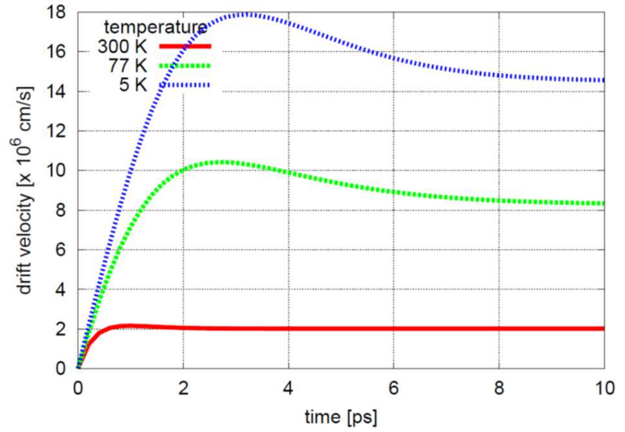

Fig. 6. Time-dependent electron drift velocity curves were obtained for 5 (blue line), 77 (green), and 300 K (red). Only phonon scattering is considered. Even at low-temperature conditions with small phonon scattering probabilities, smooth velocity overshoot characteristics are obtained by the present method.

Fig. 7 shows the temperature-dependent electron mobility with and without interface roughness scattering considerations for the GaN channel layer thicknesses of 10 and 30 nm. For the interface roughness scattering parameters, the roughness amplitude Δ of 0.5 nm, and the characteristic length L of 1.6 nm are used for both channel thickness cases. At room temperature, even when interface roughness scattering is not considered, mobility decreases when the GaN layer thickness becomes thinner. This is because phonon scattering increases when electron confinement becomes narrower, and this tendency becomes ambiguous at low temperatures where phonon scattering decreases. On the other hand, when the interface roughness scattering is taken into consideration, the interface roughness scattering becomes dominant at low temperatures, and the influence of the GaN thickness is also mainly caused by the interface roughness scattering at low temperatures. The interface roughness scattering also decreases the mobility at room temperature as discussed in Fig. 6. Thus, the method helps to understand the temperature-dependent mobility obtained by Hall measurements.

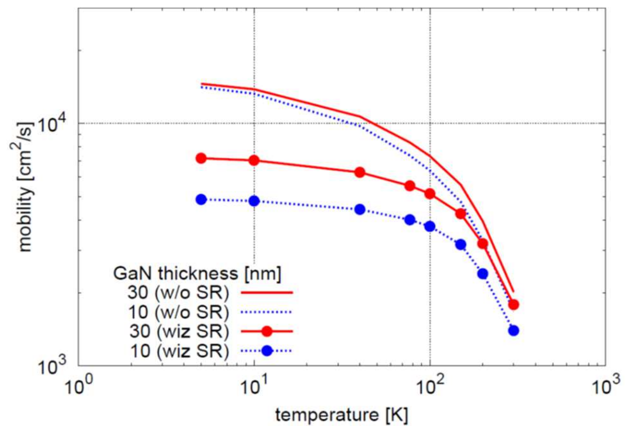

Fig. 7. Obtained temperature dependence of HEMT electron mobility, with and without interface roughness scattering consideration, for the GaN channel layer thicknesses of 10 and 30 nm.

Fig. 8 shows the energy-dependent scattering rates of the first subband electron caused by acoustic, optical, polar optical phonons and interface roughness scattering for the 30 nm GaN thickness device, a) is for 300 K and b) is for 5 K. The phonon scattering rate is gradually increased by the electron energy because of the band nonparabolicity consideration. While acoustic phonon is reduced drastically at 5K, the interface roughness rate is not changed so much. Optical and polar optical phonon scattering rates are more complicated, the emission rate which is major above 0.1 eV is almost the same for both temperatures, while the absorption below 0.1 eV differs much. Even though, since the electron above 0.1 eV is rare at 5 K, the total phonon scattering rate is drastically reduced at 5 K.

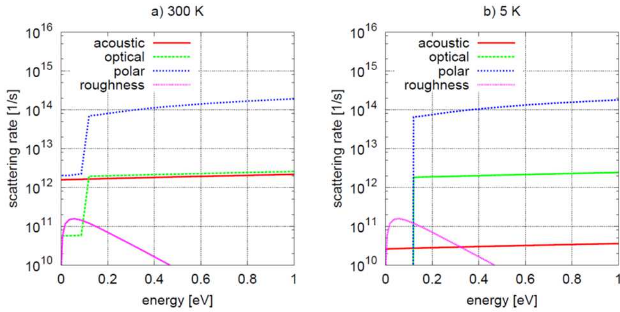

Fig. 8. Energy-dependent scattering rates in the 30 nm GaN thickness device at a) 300 K and b) 5 K. At 5 K, phonon scattering is reduced, and interface roughness scattering remains.

Fig. 9 shows the same figure as Fig. 8 but for the 10 nm GaN thickness device. The acoustic and optical phonon scattering rates are increased compared with the 30 nm case in Fig. 8, because of the increase of the overlap integral values in the scattering models, caused by the stronger confinement. The polar optical phonon does not change so much because the overlap integral is multiplied by the exponential function of the distance between two depth points. Even the same interface roughness parameters are used, the roughness scattering is increased because of the steeper conduction band slope of the 10 nm case which strengthens the effect of the interface roughness.

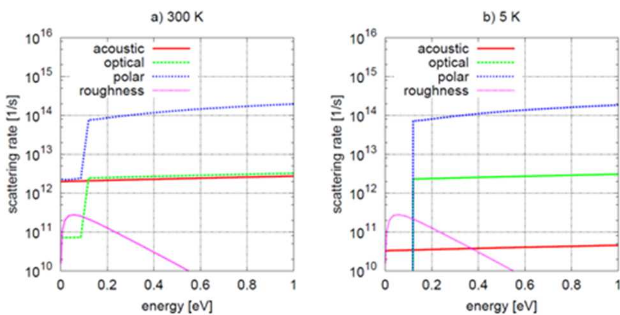

Fig. 9. Energy-dependent scattering rates in the 10 nm GaN thickness device at a) 300 K and b) 5 K.At 5 K, phonon scattering reduces, and interface roughness scattering remains.

From Fig. 7 to Fig. 9, the essence of physics of the temperature dependence of the low field mobility of the GaN HEMTs is well understood. The too-thin GaN channel layer degrades the low field mobility because of the increase of the phonon scattering caused by the increase of the overlap integrals, and the interface roughness scattering caused by the increase of the conduction band slope. Both are critical at the room temperature of 300 K. The present combined method of the Poisson-Schrodinger and the cellular automaton is the strong mobility modeling tool that helps the channel design of HEMTs.

IV. Conclusions

The temperature dependence of HEMT mobility was investigated by a combined approach of the Poisson-Schrodinger method and the cellular automaton method. It is confirmed that stable solutions are obtained seamlessly even at low temperatures. The temperature dependence of mobility for different thicknesses of HEMT GaN layers was studied using the present method. As a result, it is quantitatively predicted that interface roughness scattering predominates at low temperatures. This method also predicts that phonon scattering is increased and mobility is decreased when the GaN channel thickness becomes too thin.

Acknowledgment

This work was partially supported by Innovative Science and Technology Initiative for Security Grant Number JPJ004596, ATLA, Japan.

References

[1] T. Ohki, A. Yamada, Y. Minoura, K. Makiyama, J. Kotani, S. Ozaki, and N. Nakamura, “An over 20-W/mm S-band InAlGaN/GaN HEMT with SiC/diamond-bonded heat spreader,” IEEE Electron Device Lett., vol. 40, no. 2, pp. 287-290, 2019.

[2] C. Jungemann, A. Emunds, and W. L. Engl, “Simulation of linear and nonlinear electron transport in homogeneous silicon inversion layers,” Solid-State Electron., vol. 36, no. 11, pp. 1529-1540, 1993.

[3] K. Fukuda, J. Hattori, H. Asai, J. Yaita, and J. Kotani, “A continuous cellular automaton method with flux interpolation for two-dimensional electron gas electron transport analysis,” in Proc. SISPAD, pp. 55-58, 2020.

[4] K. Fukuda, J. Hattori, H. Asai, J. Yaita, and J. Kotani, “A Poisson–Schrodinger and cellular automaton coupled approach for two-dimensional electron gas transport modeling of GaN-based high mobility electron transistors,” Jpn. J. Appl. Phys, vol. 60, 2021.

[5] B. E. Foutz, S. K. O’Leary, M. S. Shur, and L. F. Eastman, “Transient electron transport in wurtzite GaN, InN, and AlN,” J. Appl. Phys., vol. 85, no. 11, pp. 7727-7734, 1999.

[6] M. Farahmand, C. Garetto, E. Bellotti, K.F. Brennan, M. Goano, E. Ghillino, and. P. P. Ruda, “Monte Carlo simulation of electron transport in the III-nitride wurtzite phase materials system: binaries and ternaries,” IEEE Trans. Electron Devices, vol. 48, no. 3, pp. 535-542, 2001.

[7] S. Yamakawa, E. Ueno, K. Taniguchi, C. Hamaguchi, K. Miyatsuji, K. Masaki, and U. Ravaioli, “Study of interface roughness dependence of electron mobility in Si inversion layers using the Monte Carlo method,” J. Appl. Phys., vol. 79, no. 2, pp. 911-916, 1996.

[8] S. Patwal., M. Agrawal., K. Radhakrishnan., T.L.A. Seah, and N. Dharmarasu, ”Enhancement of 2D Electron Gas Mobility in an AlN/GaN/AlN Double-Heterojunction High-Electron-Mobility Transistor by Epilayer Stress Engineering,” Phys. Status Solidi A, vol. 217, 1900818, 2020.

[9] K. Fukuda and K. Nishi,” An interpolated flux scheme for cellular automaton device simulation,” IEEE Trans. CAD, 17, pp. 553–560 1998.